Materials Science & Engineering C 131 (2021) 112521

Contents lists available at ScienceDirect

Materials Science & Engineering C

journal homepage: www.elsevier.com/locate/msec

Effective and prolonged targeting of a nanocarrier to the inflammation site by functionalization with ZnBPMP and chitosan

Kiyoon Min [a], Soyeon Yoo [b], Min Su Han [b,*], Giyoong Tae [a,*]

[a] School of Materials Science and Engineering, Gwangju Institute of Science and Technology (GIST), Gwangju 61005, Republic of Korea
[b] Department of Chemistry, Gwangju Institute of Science and Technology (GIST), Gwangju 61005, Republic of Korea

ARTICLE INFO

Keywords:
Inflammation
Nanocarrier
ZnBPMP
Chitosan
Skin hypersensitivity

ABSTRACT

Efficient and selective targeting of inflamed tissues/organs is critical for diagnosis and therapy. Although nanomaterials themselves have an intrinsic advantage due to their size for targeting inflammation sites, additional functionalization of the nanomaterials with proper targeting moieties is desired to enhance the targeting efficiency. In this study, we aimed to improve the inflammation targeting characteristics of a pluronic-based nanocarrier, which has advantages as a nanosized delivery cargo for diverse molecules, by conjugating with chitosan and ZnBPMP (two Zn(II) ions chelated 2,6-bis[(bis(2-pyridylmethyl)amino)-methyl]-4-methylphenol) moiety. Specific and significant cellular uptake and interaction between the nanocarrier functionalized with ZnBPMP ligand and chitosan to an apoptosis-induced immune cell line were observed *in vitro*. An inflammation model in the mouse ear caused by skin hypersensitivity was used to evaluate the effect of functionalization with chitosan and ZnBPMP moiety by comparing with various control groups. Functionalization of the nanocarrier with chitosan greatly enhanced the *in vivo* circulation time of the nanocarrier, so prolonged targeting ability of the nanocarrier to the inflamed ear was achieved. Additional ZnBPMP functionalization to chitosan-functionalized nanocarrier also resulted in significantly improved initial targeting and further enhancement in the targeting until 5 days to the inflamed ear and the decreased non-specific accumulation of the nanocarrier to the remaining body. Thus, developed nanocarrier has a high potential as a drug delivery carrier as well as a diagnostic agent to the inflammation sites.

1. Introduction

Inflammation, one of the important causes of many diseases, such as microbial infections, metabolic disorders, cardiovascular diseases, neurological diseases, and even cancers, can be fatal or intimate to our lives [1–3]. Diagnosis or detection of the inflammation in advance can prevent the diseases from becoming worse and severe. Accordingly, the development of sensitive and accurate systems for detecting inflammation is important and practical in biomedical applications. Nanomaterials have been extensively used for inflammation detective systems. For example, polymeric nanoparticles showed targeting and delivery of loaded drugs to the inflammation site [4,5]. Micelles [6], liposomes [7], and metal-based nanoparticles [8] have also been actively studied for the same purposes. These systems passively relied on their nanosize for targeting based on the angiogenesis at the inflammation site without active targeting characteristics. Various targeting strategies for active targeting to the inflammation site were also developed. Kim et al. utilized caspase families, which are activated by inflammation [2,9]. On the other hand, macrophages near the inflamed site have been utilized as a target of the nanoparticles [10]. The pH difference between normal and inflamed tissues [6] and the specific cytokine in the inflammatory environment [11] could be other strategies. However, nanosystems satisfying both characteristics of efficient and selective targeting for diagnosis of the inflamed site and long-term residence at the target site for the therapeutic effect of loaded drugs have not been well studied.

Zinc(II)-dipicolylamine (ZnDPA) is known as a targeting ligand to phosphatidylserine (PS) on the external cell membrane, mimicking Annexin V protein [12,13]. PS is known to be abundant on the surface of the membrane of bacteria, apoptotic/necrotic cells, inflamed cells, and cancer cells [12–14]. Zn^{2+} ions coordinated in ZnDPA have an affinity to the head group of anionic phospholipids. In previous studies, ZnDPA was conjugated directly to small molecular weight active agents such as dyes [12–14] or drugs [15] and showed successful targeting to dead

* Corresponding authors.
E-mail addresses: happyhan@gist.ac.kr (M.S. Han), gytae@gist.ac.kr (G. Tae).

https://doi.org/10.1016/j.msec.2021.112521
Received 29 June 2021; Received in revised form 19 October 2021; Accepted 22 October 2021
Available online 26 October 2021

cells, tumors, and arthritis sites as well as a therapeutic effect. Furthermore, ZnDPA modification to nanoparticle encapsulating iron oxide was used to separate bacteria magnetically [16], and ZnDPA conjugation to iron oxide nanoparticles could amplify magnetic resonance signal and photothermal therapy on tumor site [17]. A 2,6-bis [(bis(2-pyridylmethyl)amino)-methyl]-4-methylphenol (BPMP) is a ligand that contains two DPA moieties in one molecule and has the property of coordinating to dinuclear metal ions, such as Mn^{2+}, Zn^{2+}, and Ni^{2+} ion [18,19]. ZnBPMP, with two coordinated Zn^{2+} ions, showed selectively high binding affinity to various phosphate-containing biomolecules such as ATP and phospholipids, applicable for sensor or imaging tools targeting phosphate-containing biomolecules [20–24]. The binding affinity of di-ZnDPA-based ligands like ZnBPMP to phosphate ions is about 10 to 100 times higher than that of mono-ZnDPA based ligands [22,25–27]. ZnBPMP also has phenoxide between two ZnDPA moieties, so it holds a structure capable of binding to phosphate ions [28]. Thus, ZnBPMP has a high potential to act as a more selective ligand to inflammatory cells with sufficient PS on the outer surface.

Pluronic is a tri-block copolymer, which consists of poly(ethylene oxide)-poly(propylene oxide)-poly(ethylene oxide) (PEO-PPO-PEO). Especially, pluronic F68 (PEO 76 PPO 29 PEO 76, MW 8400) has been widely used to prepare drug delivery carriers and hydrogels for biomedical applications due to its biocompatibility, thermosensitive gelation characteristic [29–31]. For example, we previously reported that pluronic-based nanocarrier, which has advantages for nanocarriers including nano size (~100 nm) in physiological condition, biocompatibility, and simple and very efficient loading of diverse molecules, such as proteins [32,33], small molecules [34], and metal nanoparticles [33,35], while maintaining the activity of loaded biomolecules. Chitosan functionalization to the nanocarrier further increased the cellular uptake, tumor-targeted accumulation, and skin permeability [36,37]. So, by attaching pH-sensitive fluorescence dye, chitosan-functionalized, pluronic-based nanocarrier could be used for selective imaging of the inflammation site [38]. We also demonstrated that the additional conjugation of selective ligand to chitosan-functionalized, pluronic-based nanocarrier showed the synergistically enhanced targeted delivery to the brain [39] and oral delivery [40]. So, based on these previous studies, we aimed to develop a nanosystem that has high selectivity and longevity to a target inflammation site in this study by functionalization with chitosan and conjugation of ZnBPMP moiety to the pluronic-based nanocarrier (Scheme 1). It was hypothesized that the synergistic effect of chitosan providing long blood circulation and ZnBPMP moiety would improve the targeting efficiency to the inflammation site. To the best of our knowledge, the conjugation of ZnBPMP (or ZnDPA) ligand to nanocarrier instead of direct conjugation to small molecular weight drugs or dyes for *in vivo* targeting has not been reported. By improving targeting properties of delivery carriers, various drugs can be delivered efficiently using the same vehicle, and loss of activity of drugs does not need to be considered. Apoptosis-induced Jurkat cell line and the skin hypersensitivity model were used to analyze and compare the targeting efficiency of pluronic-based nanocarriers with various modifications to the inflammation site.

2. Materials and methods

2.1. Materials

Pluronic F68 (PF68) (PEO 76 PPO 29 PEO 76, MW 8400) was kindly donated from BASF Corporation (Seoul, Korea). Chitosan (7 kDa) was obtained from Amicogen (Jinju, Korea). Acryloyl chloride, triethylamine, zinc nitrate, ninhydrin reagent, acetone, and olive oil, fluorescein isothiocyanate (FITC) were obtained from Sigma-Aldrich (St. Louis, MO, USA). Irgacure 2959 and cyanine 5.5 (cy 5.5) NHS ester were bought from Ciba Specialty Chemicals (Basel, Switzerland) and Lumiprobe (Hunt Valley, MD, USA), respectively. Thionyl chloride, 3-(4-hydroxyphenyl)propanoic acid, di(2-picolyl)amine, methyl 3-(4-hydroxyphenyl)propanoate, lithium hydroxide, N-(3-dimethyl aminopropyl)-N′-ethyl carbodiimide hydrochloride, N-hydroxysuccinimide, zinc nitrate, paraformaldehyde, chloroform, methanol, tetrahydrofuran, and acetonitrile for BPMP conjugated chiNC were bought from Sigma-Aldrich, Tokyo Chemical Industry (Tokyo, Japan), and Alfa Aesar (Haverhill, MA, USA). Jurkat cell line was obtained from the Korean cell line bank (Seoul, Korea). Roswell Park Memorial Institute (RPMI) 1640 media, fetal bovine serum (FBS), antibiotic-antimycotic (AA), and Annexin V (Alexa Fluor™ 488 conjugate) were purchased from ThermoFisher (Waltham, MA, USA). Camptothecin (CPT) was bought from Tokyo Chemical Industry. Cell Counting Kit-8 (CCK-8) was purchased from Dojindo Laboratories (Kumamoto, Japan). C67BL/6 mice (5 weeks, male) were bought from G-bio (Gwangju, South Korea). 1-Fluoro-2,4-dinitrobenzene (DNFB) was obtained from Alfa Aesar.

2.2. Synthesis of chitosan functionalized nanocarrier

Bare PF68 nanocarrier (bareNC) and chitosan-functionalized PF68 nanocarrier (chiNC) were synthesized as previously reported [29,36]. First, diacrylate PF68 and glycidyl methacrylated chitosan were prepared. For making diacrylated PF68, 5 g of PF68 was dissolved in 50 mL of toluene. Then, 0.83 mL of triethylamine and 0.49 mL of acryloyl

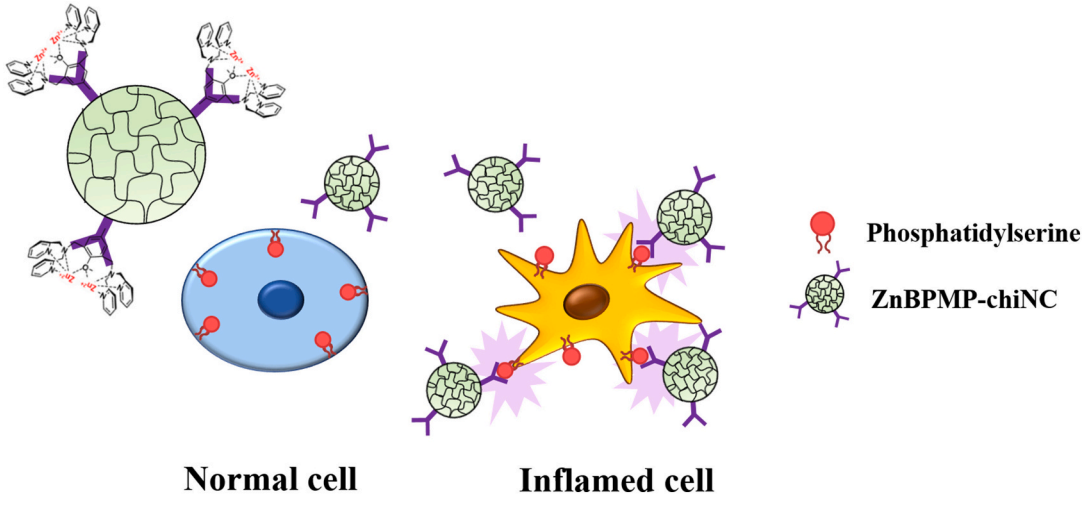

Scheme 1. Selective targeting of a nanocarrier to the inflammation site by functionalization with chitosan moiety and ZnBPMP having an affinity to phosphatidylserine, which is exposed to the surface of the inflamed cell membrane.

chloride were added to proceed overnight reaction. The reacted solution was precipitated using ethyl ether and dialyzed using an MWCO 3.5 kDa dialysis membrane for two days against deionized water (DIW) for further purification. The final solution was freeze-dried and kept at −20 °C until further use. Glycidyl methacrylated chitosan was prepared by reacting 1 g of chitosan and 0.106 mL of glycidyl methacrylate in DIW. After overnight reaction in a dark condition, the solution was precipitated in acetone, dialyzed using an MWCO 3.5 kDa dialysis membrane against DIW for 2 days, and freeze-dried.

Bare and chitosan-functionalized nanocarriers were prepared by photo-crosslinking using a 365 nm UV lamp (1.3 mW/cm^2, VL-4.LC, 8 W, Viber Lourmat, France). For the synthesis of bareNC, 10 mg of diacrylated PF68 was dissolved in 2 mL of DIW, and Irgacure 2595 as photo-initiator was added as 0.09 wt% of the final volume. Then, UV irradiation was applied for 15 min. ChiNC was synthesized by the same method with the additional input of 2.8 mg of GMA-chitosan. Synthesized nanocarrier was dialyzed (MWCO 50 kDa) against DIW for 2 days and freeze-dried, and the chitosan content was measured by a ninhydrin assay.

2.3. Preparation of ZnBPMP-chiNC

BPMP was synthesized in three steps according to the previous report [41]. Detailed experimental procedure and NMR data were provided in the supplementary material and Fig. S1. BPMP was conjugated to chiNC using EDC coupling. The mixture of BPMP having a carboxylic acid group (0.22 mmol, 0.13 g), N-(3-dimethylaminopropyl)-N′-ethyl-carbodiimide hydrochloride (EDCI; 1.12 mmol, 0.21 g), and N-hydroxysuccinimide (NHS; 1.12 mmol, 0.13 g) in 100 mL of acetonitrile was stirred for 2 h. ChiNC (0.51 g) in 250 mL of DIW was added dropwise to the above mixture, and then the mixture was stirred for 1 day. The mixture was dialyzed in acetonitrile: DIW = 1:4 for two days and in DIW for an additional one day. Dried BPMP-chiNC was obtained by freeze-drying.

The final form of ZnBPMP-chiNC was prepared by incubating BPMP-chiNC with 2 equivalents of zinc nitrate for BPMP at room temperature for 15 min before use.

2.4. Characterization of nanocarriers

The size and zeta potential of nanocarriers were measured using dynamic light scattering (DLS, ELSZ-2000, Otsuka Electronics, Osaka, Japan). Each bareNC, chiNC, and BPMP-chiNC were dissolved in PBS for measurements. The sizes of bareNC, chiNC, and BPMP-chiNC were measured at 4, 25, and 37 °C to see their thermo-sensitivity. The final form ZnBPMP-chiNC used for the *in vivo* targeting was prepared by chelating BPMP-chiNC with Zn^{2+} and the size of it was measured at 37 °C. The nanocarriers were dissolved in DIW and prepared in the same way for zeta potential measurement. The morphologies of newly developed BPMP-chiNC and ZnBPMP-chiNC incubated at 37 °C were observed by a transmission electron microscope (TEM, Tecnai G2 S-Twin, FEI, OR, USA).

2.5. Colloidal stability of nanocarriers

The colloidal stability of nanocarriers in the serum environment was observed by measuring the size change of the nanocarriers over time. Nanocarriers were dissolved in phosphate-buffered saline (PBS, pH 7.4) containing 10% of FBS and 0.05% of sodium azide. The nanocarrier solutions were sealed and incubated at 37 °C, and the sizes of nanocarriers were measured at pre-determined time points.

2.6. In vitro experiments

Jurkat cells were cultured in RPMI media with 10% of FBS and 1% of AA under 5% CO_2 at 37 °C. 10,000 cells/well were seeded on a well plate and various concentrations of the nanocarriers were treated. After 24 h, CCK-8 reagent was added and incubated for 30 min. The absorbance of the reagent-added media was measured using a microplate reader (Varioskan Lux, ThermoFisher, Waltham, MA, USA) at 450 nm.

For cellular uptake observation, the nanocarriers were conjugated with FITC and cy 5.5-NHS ester. 10 mg of the nanocarriers (bareNC, chiNC, and BPMP-chiNC) dissolved in 1 mL of 0.1 M sodium carbonate buffer (pH 9) and 0.1 M phosphate buffer (pH 8) for each reaction were mixed with 75 μg of FITC and 16.7 μg of cy 5.5-NHS ester dissolved in DMSO, respectively. The reaction proceeded under 200 rpm overnight. The reacted solution was dialyzed using a 50 kDa of dialysis membrane against DIW for 48 h and freeze-dried for further experiment. ZnBPMP-chiNC was prepared by chelation of Zn^{2+} with FITC/cy 5.5-conjugated BPMP-chiNC for 15 min before treatment (Scheme S1).

100,000 cells/well were seeded on a well plate with/without 10 μM of CPT and incubated for 24 h at 37 °C. Various FITC-labeled nanocarriers were treated to the cells with a final 0.5 mg/mL concentration and incubated for 24 h. The cells were collected and centrifuged under 1500 rpm for 3 min. The supernatant media was suctioned and the cells were washed with PBS. The washed cells were again collected by centrifugation and dispersed in RPMI for a confocal laser scanning microscopy (CLSM, FV1000, Olympus, Tokyo, Japan) imaging.

The binding interaction between the nanocarriers and the apoptosis-induced cells *via* phosphatidylserine was analyzed *in vitro*. The Jurkat cells were seeded in the same way as the cellular uptake experiment. After treating with CPT for 24 h, the cy5.5-labeled nanocarriers were added as the final concentration of 0.5 mg/mL. Then, the cells were incubated at 4 °C for 4 h to minimize the cellular uptake. Annexin V (Alexa 488 conjugate) was stained for 15 min. Then, the cells were washed with PBS and imaged by the CLSM. The quantification of the fluorescence intensity from the fluorescent images was analyzed using ImageJ software after subtracting the background signal from the specific fluorescence signals.

2.7. Skin hypersensitivity model

A skin hypersensitivity model was established to analyze the targeting ability of nanocarriers to the inflammation site using C67BL/6 mice. The animal experiment in this study was approved by the Animal Care and Use Committee of Gwangju Institute of Science and Technology (GIST-2020-114). DNFB (0.2%) was dissolved in acetone:olive oil = 4:1 co-solvent. The co-solvent without DNFB was also prepared for the control. The mice were anesthetized using isoflurane in the air-way, and 20 μL of co-solvent with and without DNFB was painted on the dorsal part of the left and right ear, respectively. The ears were painted 3 times at the time points described in Fig. 3 (a).

The thicknesses of the inflamed (left) ear and the control (right) ear were measured using a Vernier Caliper (Mitutoyo, Kanagawa, Japan) to analyze the occurrence of inflammation. The ear skin tissues at day 0 and day 5 were extracted and fixed in 10% of formalin. The tissue was embedded in an optimal cutting temperature compound (OCT) and sectioned at 10 μm thickness using a cryotome (Leica, Wetzlar, Germany). Tissue slices were stained with hematoxylin and eosin Y (H&E) for histological analysis. The stained images were observed using an optical microscope (TE2000-U, Nikon Co., Tokyo, Japan).

2.8. Inflammation targeting of nanocarriers

Skin hypersensitivity-induced mice were randomly grouped for four types of nanocarriers: bareNC, chiNC, BPMP-chiNC, and ZnBPMP-chiNC. The cy5.5-labeled nanocarriers were used for the *in vivo* experiment. ZnBPMP-chiNC was prepared by chelation of Zn^{2+} with cy 5.5-conjugated BPMP-chiNC for 15 min before injection (Scheme S1). The nanocarriers and zinc nitrate solution were filtered with a 0.2 μm nylon syringe filter. 1 mg of nanocarrier in 200 μL of 0.9% saline was prepared and intravenously (*i.v.*) injected into a mouse tail vein. FOBI

(Fluorescence *In Vivo* Imaging System, NeoScience, Seoul, Korea) was used for *in situ* fluorescence imaging for biodistribution of the nanocarriers for 3 days after injection. The mice were sacrificed on day 5, and each left and right ear and major organs (liver, kidney, spleen, lung, and heart) were extracted for measurement of organ distribution of the nanocarriers. All data were plotted in total intensity.

2.9. Statistical analysis

All data were analyzed by Student's *t*-test or ANOVA (Analysis of variance). *p*-value under 0.05 was regarded to be significantly different. ($^{\#}$: $p > 0.05$ no significance difference, *: $p < 0.05$, **: $p < 0.01$, ***: $p < 0.001$).

3. Results and discussion

3.1. Preparation and characterizations of nanocarriers with various functionalizations

The nanoparticle system for targeting the inflammation site was developed by conjugating ZnBPMP moiety to chitosan-functionalized pluronic-based nanocarrier. To demonstrate the synergetic effect of chitosan and ZnBPMP, various nanoparticles were synthesized for systemic comparison (Fig. 1 (a) and Fig. S2). BareNC without chitosan and ZnBPMP modification, chiNC with only chitosan functionalization (14.5 ± 1.6 wt% of chitosan content), BPMP-chiNC with BPMP conjugation to chiNC but without Zn^{2+} ion chelation, and ZnBPMP-chiNC with both chitosan and ZnBPMP (Zn^{2+} ion chelated BPMP) were prepared. Both bareNC and chiNC were previously reported by our group, showing ~150 nm in size at 37 °C with very large thermal expansion at low temperatures [36]. Conjugation of BPMP moiety to chiNC by reacting carboxyl groups of BPMP with amine groups of chitosan of chiNC using EDC coupling was also reported by us [19]. However, nanocarriers made of a different kind of pluronic (PF 127 instead of PF 68) were used and Mn^{2+} ion was chelated instead of Zn^{2+} ion to utilize peroxidase-mimicking properties of MnBPMP in that report. The conjugation of BPMP to chiNC (BPMP-chiNC) was confirmed by ^{1}H NMR spectrum, showing the aromatic ring of BPMP at around 7.0–8.5 ppm and propyl group of pluronic at around 1.0 ppm (Fig. 1 (b)). Based on NMR data, 7.28 μM of BPMP was conjugated in 1 mg/mL of BPMP-chiNC, meaning that one BPMP molecule was conjugated per 1.5 chitosan chains. Zn^{2+} chelation to BPMP-chiNC to get ZnBPMP-chiNC was processed before use. We also prepared BPMP-bareNC (BPMP conjugated to bareNC) after amine functionalization of bareNC following the previous report [36] to observe the effect of ZnBPMP only. As a result, 7.67 μM of BPMP was conjugated to 1 mg/mL of BPMP-bareNC, which showed a similar conjugation ratio of BPMP to that of BPMP-chiNC (data not shown). However, BPMP-bareNC was not stable in an aqueous environment. It did not maintain the nanosize with a relatively narrow distribution, but induced aggregation among them, probably mediated by the hydrophobicity of BPMP. Thus, we could systematically compare bareNC, chiNC, BPMP-chiNC, and ZnBPMP-chiNC excluding BPMP-bareNC for inflammation targeting ability.

Physicochemical properties of prepared nanocarriers were analyzed. Sizes at different temperatures and zeta potentials of the nanocarriers were measured by DLS, as shown in Fig. 2 (a) and (b). The sizes of bareNC at 37, 25, and 4 °C were 153 ± 8, 258 ± 22, and 336 ± 14 nm, respectively, and chiNC also showed 168 ± 19, 246 ± 30, and 369 ± 20

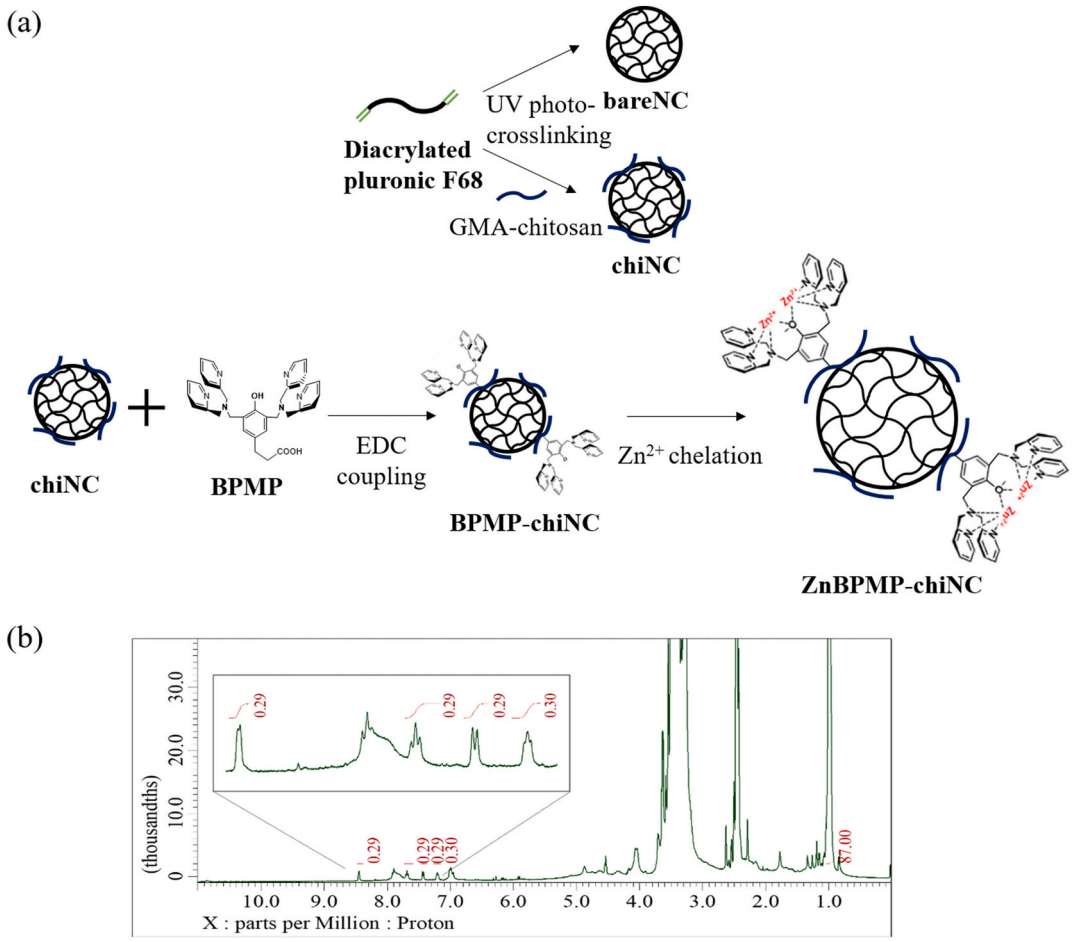

Fig. 1. (a) Synthesis of various nanocarriers (bareNC, chiNC, BPMP-chiNC, and ZnBPMP-chiNC). (b) ^{1}H NMR spectrum of BPMP-chiNC.

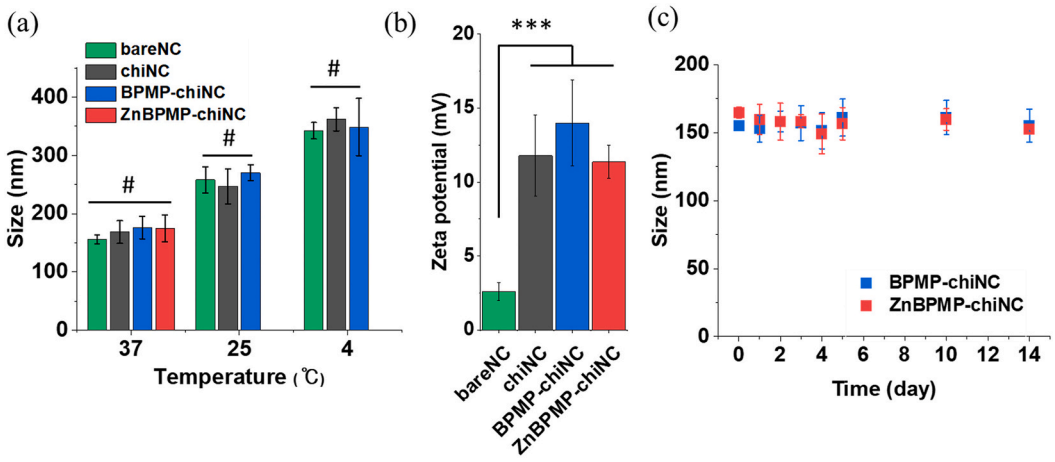

Fig. 2. Physicochemical properties of the nanocarriers. (a) Size at various temperatures and (b) zeta potential of various nanocarriers. (c) *In vitro* colloidal stability of the nanocarriers under 10% serum condition for two weeks. (#: $p > 0.05$, ***: $p < 0.001$).

nm in size at each temperature. The results well coincided with our previous report [36], showing a large thermal sensitivity with nano-sizes at the physiological condition. Even after conjugation of very hydrophobic BPMP moiety to chiNC, the size of BPMP-chiNC did not change significantly, showing 176 ± 19, 270 ± 13, and 349 ± 49 nm at 37, 25, 4 °C. This result suggests that various molecules can be loaded into the nanocarrier using this thermo-sensitivity for further therapeutic applications.

In terms of surface charge, a neutral charge state of bareNC (2.6 ± 0.6 mV) became positive after chitosan conjugation due to the positively charged chitosan (11.8 ± 2.7 mV of chiNC), as previously reported [36]. However, BPMP conjugation did not cause any meaningful change to the surface charge (14.0 ± 2.9 mV of BPMP-chiNC). Notably, chelation with Zn^{2+} ion did not cause any change to the size (174.7 ± 23 nm at 37 °C) or surface charge (11.4 ± 1.1 mV) of the nanocarrier. The TEM images of BPMP-chiNC and ZnBPMP-chiNC showed their spherical nano-sized morphologies, similar to previously reported bareNC and chiNC [42], with similar sizes obtained from DLS analysis (Fig. S2). Thus, the main physicochemical properties (size and surface charge) of pluronic-based nanocarrier were preserved after BPMP functionalization and additional chelation with Zn^{2+} ion, so the difference in targeting ability to the inflammation site must result from the difference in surface functionalities.

After intravenous administration of nanocarriers *in vivo*, they need to maintain their nano-sizes without aggregation or precipitation for long circulation to have their targeting ability. So, the colloidal stability of BPMP-chiNC and ZnBPMP-chiNC was analyzed by incubating nanocarriers in a 10% serum-containing media at 37 °C (Fig. 2 (c)). The size changes of the nanocarriers were monitored at each time point using DLS. Good serum stability of bareNC and chiNC was already reported in our previous study [36]. BPMP-chiNC and ZnBPMP-chiNC were additionally measured for two weeks, also revealing no aggregation formation. Thus, it was verified that the nanocarriers with various surface functionalities would maintain colloidal stability in physiological conditions.

3.2. Cellular uptake and binding affinity between the nanocarriers and the apoptosis-induced Jurkat cells in vitro

Jurkat cell line is a human T lymphoblast, which has been commonly used for the Annexin V and apoptosis experiments, as well as the study showing the binding affinity between ZnDPA and phosphatidylserine [12,43]. CPT, an anticancer drug, was treated to the cells to induce apoptosis. The apoptosis-induced T lymphoblast has highly related to the inflammation since the inflammation environment recruits T lymphocytes and induces apoptosis [44]. So, the Jurkat cell was chosen for the *in vitro* experiments. First, the cytotoxicity of various nanocarriers to Jurkat cells was analyzed. All nanocarriers showed no sign of cytotoxicity even at the high concentration (1 mg/mL) of the nanocarriers, as shown in Fig. S3.

Next, the cellular uptake of various nanocarriers into normal cells (CPT untreated) and apoptosis-induced cells by CPT was observed using the CLSM. The FITC-labeled nanocarriers were incubated with the cells for 24 h at 37 °C to be uptaken. The untreated group showed little fluorescence signal in all groups, revealing little cellular uptake with no significant differences among the nanocarriers. However, by CPT treatment, although increased cellular uptake was observed for all groups, ZnBPMP-chiNC showed distinctively and dramatically increased cellular uptake (Fig. 3 (a) and (c)). It is likely that the significantly high cellular uptake of ZnBPMP-chiNC resulted from the ZnBPMP ligand *via* a binding affinity with the phosphatidylserine present in the outer cell layer of cells under apoptosis.

Furthermore, to see more directly the binding interactions between various nanocarriers and the apoptosis-induced cells, the cells were cultured with the nanocarriers under the condition of suppressed cellular uptake of the nanocarriers by incubating them at 4 °C for 4 h. Then, the cells were stained with Annexin V (Alexa 488 conjugate), which has a specific binding affinity with phosphatidylserine and is used as a biomarker of cell apoptosis. The same degree of apoptosis induction was confirmed from the similar green fluorescence (Annexin V) signals for all groups, as shown in Fig. S4. However, the red fluorescence signal from the cy5.5-labeled nanocarriers was distinctively and dramatically high only for ZnBPMP-chiNC, which was mostly co-localized with the green fluorescence signal of Annexin V (Fig. 3 (b) and (d)). So, it was elucidated that not only cellular uptake but binding affinity with apoptosis-induced cells, which have abundant phosphatidylserine, were also specifically augmented with ZnBPMP ligand. In contrast, the functionalization with chitosan alone showed only a moderate increase in cellular uptake and little improvement in binding to apoptosis-induced Jurkat cells. Also, BPMP itself without Zn^{2+} did not show any distinct effect, confirming the key role of Zn ion chelation for specificity and selectivity to the targeting effect. These *in vitro* results encouraged the promising *in vivo* targeting effect of the nanocarrier with ZnBPMP ligand and chitosan to the inflammation site.

3.3. Establishment of a skin inflammation model

The skin hypersensitivity by treating DNFB induced allergic contact dermatitis on mouse ears [45,46]. DNFB was painted on the dorsal part of the left ear and co-solvent as control was also painted on the right ear

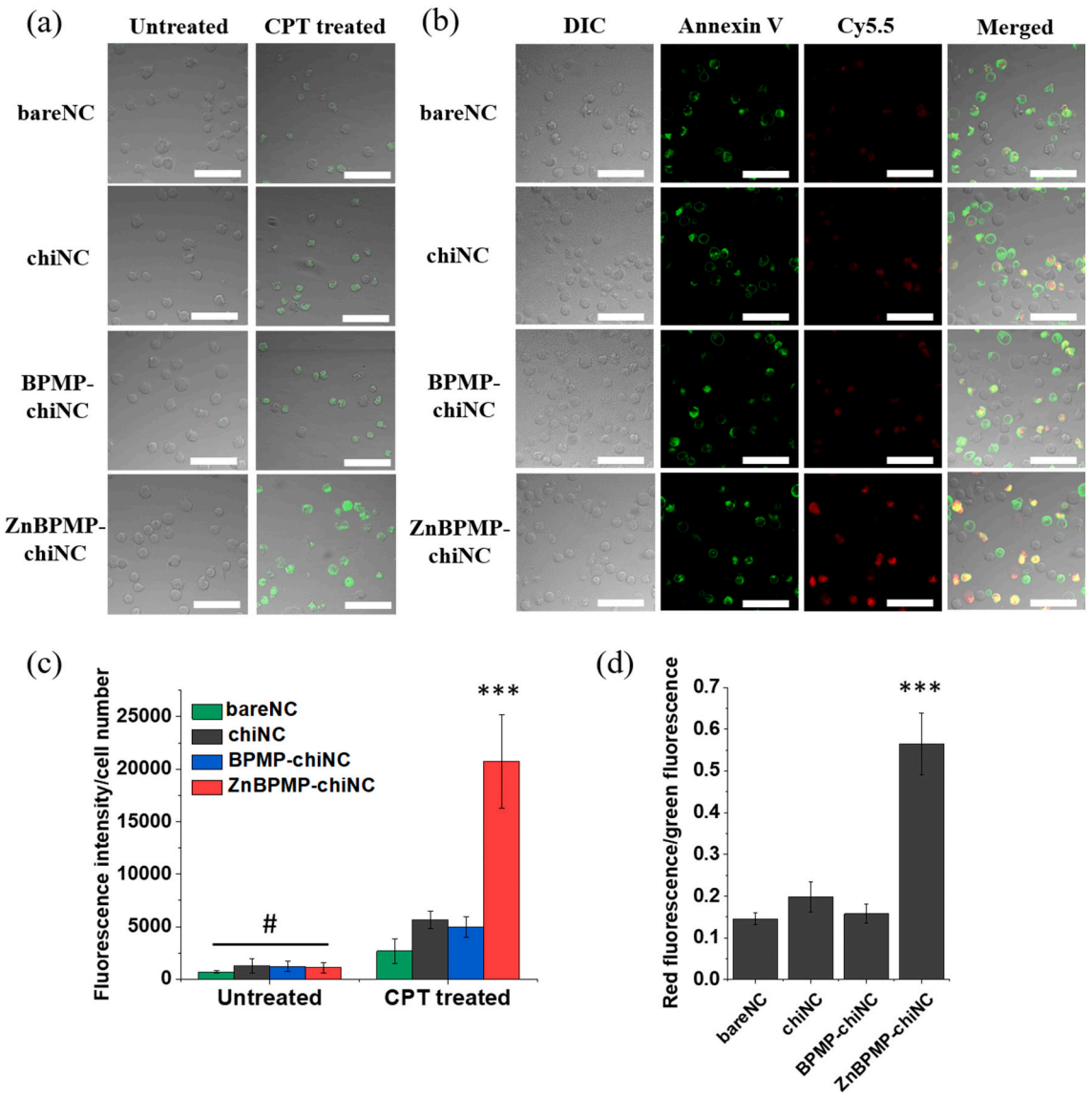

Fig. 3. (a) Cellular uptake (37 °C, 24 h) of FITC-labeled nanocarriers to Jurkat cell with and without CPT treatment. (b) Co-localization of Annexin V (Alexa 488 conjugate) and cy5.5-labeled nanocarriers on CPT-treated Jurkat cell under the condition of suppressed cellular uptake (4 °C, 4 h). Quantitative analysis of (c) the cellular uptake and (d) the interaction of the various nanocarriers with the cells. (scale bar = 50 mm) ($^{\#}$: $p > 0.05$, ***: $p < 0.001$).

for comparison. Ears were sensitized by DNFB at day −5, −4 and −1, following the schedule described in Fig. 4 (a). The ear treated with DNFB became reddish and swollen with wrinkles compared to the control ear, as shown in Fig. 4 (b). Also, the thickness of the DNFB treated ears increased over time, whereas the thickness of the control ears without DNFB showed no change (Fig. 4 (c)). The thickness of the ears showed a significant difference between the control and DNFB groups from day 0 so that the nanocarrier sample was injected on day 0. The difference in thickness between the two groups was increased almost three times on day 5, representing the allergic inflammation was in progress. Furthermore, H&E staining images in Fig. 4 (d) showed that the inflamed ears were thicker than the control ear on both day 0 and day 5. The ear tissues on day 5 became dramatically thicker than them on day 0, confirming the inflammation. Macrophages were observed as small purple dots on the DNFB treated ear. Consequently, the inflammation in the ear by DNFB treatment was properly achieved.

3.4. Targeting of nanocarriers to the inflammation site

Cy5.5 was conjugated to various nanocarriers to observe the targeting to the inflammation site as well as biodistribution of the nanocarriers after intravenous administration *via* mouse tail vein. The fluorescent intensities of labeled nanocarriers were all same, meaning that the fluorescence intensity could be used for semi-quantitative analysis of the nanocarriers. Mice were anesthetized and the fluorescence intensities of the ears were measured by a fluorescence imaging system.

The fluorescent images of various nanocarriers were monitored at several time points (Fig. 5 (a)), and the total fluorescent intensities in the region of interest (ROI) (ear) were plotted in Fig. 5 (b) and Fig. S5. First, bareNC showed a higher signal than chiNC and BPMP-chiNC without ZnBPMP at an initial time point (1 h), not only for the DNFB group but also in the control group (without inflammation), implying a high blood circulation rate of the nanosized carrier. However, bareNC was rapidly removed from both ears over time, so the signal of bareNC became lower than that of chiNC from 4 h, and the signals of bareNC became the same for both the inflamed ear and the control ear from 24 h. Most of the bareNC seemed to be cleared *in vivo* in 24 h. Thus, even with a nanosize, bareNC itself without any surface modification was not effective for targeting the inflamed site. In contrast, chiNC showed a strong signal at

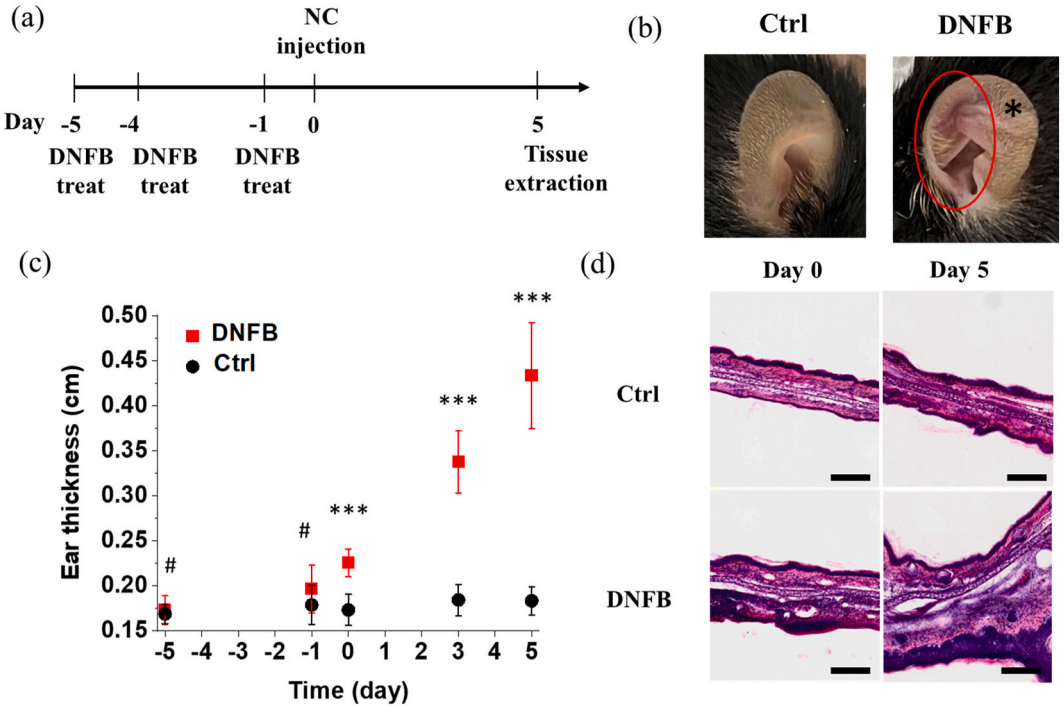

Fig. 4. (a) A schedule for establishing a mouse model with hypersensitivity ear disease using DNFB sensitization. (b) Representative ear images of the control and the DNFB group. (red circle: reddish and swollen area, *: swollen and wrinkled area). (c) Changes in ear thickness of the control and the DNFB group ($n = 9$). (d) Representative histological images of the control ear and the DNFB treated ear at day 0 and day 5 by H&E staining (scale bar = 200 μm). ($^{\#}$: $p > 0.05$, ***: $p < 0.001$). (For interpretation of the references to color in this figure legend, the reader is referred to the web version of this article.)

the inflammation site from the beginning, and the signal even increased a little up to 12 h, meaning that chiNC was accumulated to the inflammation site slowly up to 12 h. After 12 h, the signal started to decrease, but not rapidly. So, compared to the total fluorescence intensity of ROI at 12 h, over 70% of that was observed at day 3, whereas a much lower and rapid decrease of the total fluorescence intensity was observed at the control ear, showing a very distinct target (inflammation) selectivity. So, the effect of chitosan functionalization on the inflammation targeting was very clear and dramatic. The better and prolonged targeting of chiNC compared to bareNC was also observed when they were compared for tumor targeting in our previous study [36]. The homing effect of chitosan on the tumor site has been reported in several studies, and a little acidic local environment of the tumor site and pH-dependent solubility of chitosan as well as the prolonged circulation in the vascular system by chitosan functionalization were suggested as one of the plausible reasons [47,48]. The inflammation also develops a little acidic local environment [49], so the effect of chitosan functionalization on the inflammation site might be understood. In addition, using muco-adhesiveness, pH-dependent swelling, and drug release properties, chitosan has been widely used for inflammatory drug delivery [50].

By further conjugating ZnBPMP to chiNC, ZnBPMP-chiNC showed significantly more enhanced targeting characteristics. It showed the highest total fluorescence intensity among all groups from the initial time point (1 h) at the inflamed ear (DNFB). Functionalization with ZnBPMP moiety resulted in ~1.7 times higher signal compared to chiNC and BPMP-chiNC at 1 h, and the enhanced effect was maintained. Even on day 3 (72 h), ZnBPMP showed ~1.4 times higher signal than chiNC. Thus, as hypothesized, the additional effect of ZnBPMP on the inflammation targeting, mediated by the affinity of ZnBPMP to PS, was also evident and significant, although the additional enhancement by ZnBPMP was not very dramatic compared to the enhancement by chitosan functionalization alone. To analyze better the relative importance and contribution of chitosan and ZnBPMP to the targeting ability of the nanocarrier, bareNC functionalized with ZnBPMP alone needed to be compared. Even though we could prepare ZnBPMP functionalized nanocarrier without chitosan functionalization, this nanocarrier did not possess sufficient colloidal stability in physiological conditions but became aggregated easily due to the hydrophobicity of BPMP. So, it was not possible to analyze the contribution of ZnBPMP alone and compare it with other nanocarriers to the inflammation targeting. On the other hand, no meaningful difference was observed between chiNC and BPMP-chiNC (without Zn^{2+} ion chelation) at all-time points, meaning that only BPMP moiety did not have any noticeable effect on the efficiency of targeting at all, but it could augment the efficiency of targeting to the inflammation site only after chelation with Zn^{2+} ion. This result supported the role of specific affinity of ZnBPMP to PS for the inflammation targeting, not by a non-specific contribution of the BPMP moiety.

In all cases, the nanocarriers with various functionalization did not show meaningful targeting at the control ears without inflammation. Thus, it was elucidated that functionalization with chitosan and ZnBPMP has sufficient selectivity toward the inflammation site. The selectivity of nanosystems to the inflammation site compared to the normal site was explained based on the presence of newly made, premature, and sparse blood vessels at the inflammation site [51], similar to the enhanced permeability and retention (EPR) effect on the tumor site. However, the present result showed that the nanosize itself was not effective at all for the inflammation targeting, but additional functional moieties are necessary to induce the accumulation and residence of the nanocarrier at the inflammation site.

3.5. *Biodistribution of nanocarriers*

After 120 h (day 5) of injection of the nanocarriers, mice were sacrificed, and major organs were extracted. The fluorescence imaging of the extracted organs and ears *ex vivo* was taken to get the biodistribution of various nanocarriers. Fig. 6 (a) displayed the fluorescent images of the ears with or without DNFB treatment and major organs (liver, kidney, spleen, lung, and heart), and the total intensities from tissues and organs were plotted in Fig. 6 (b).

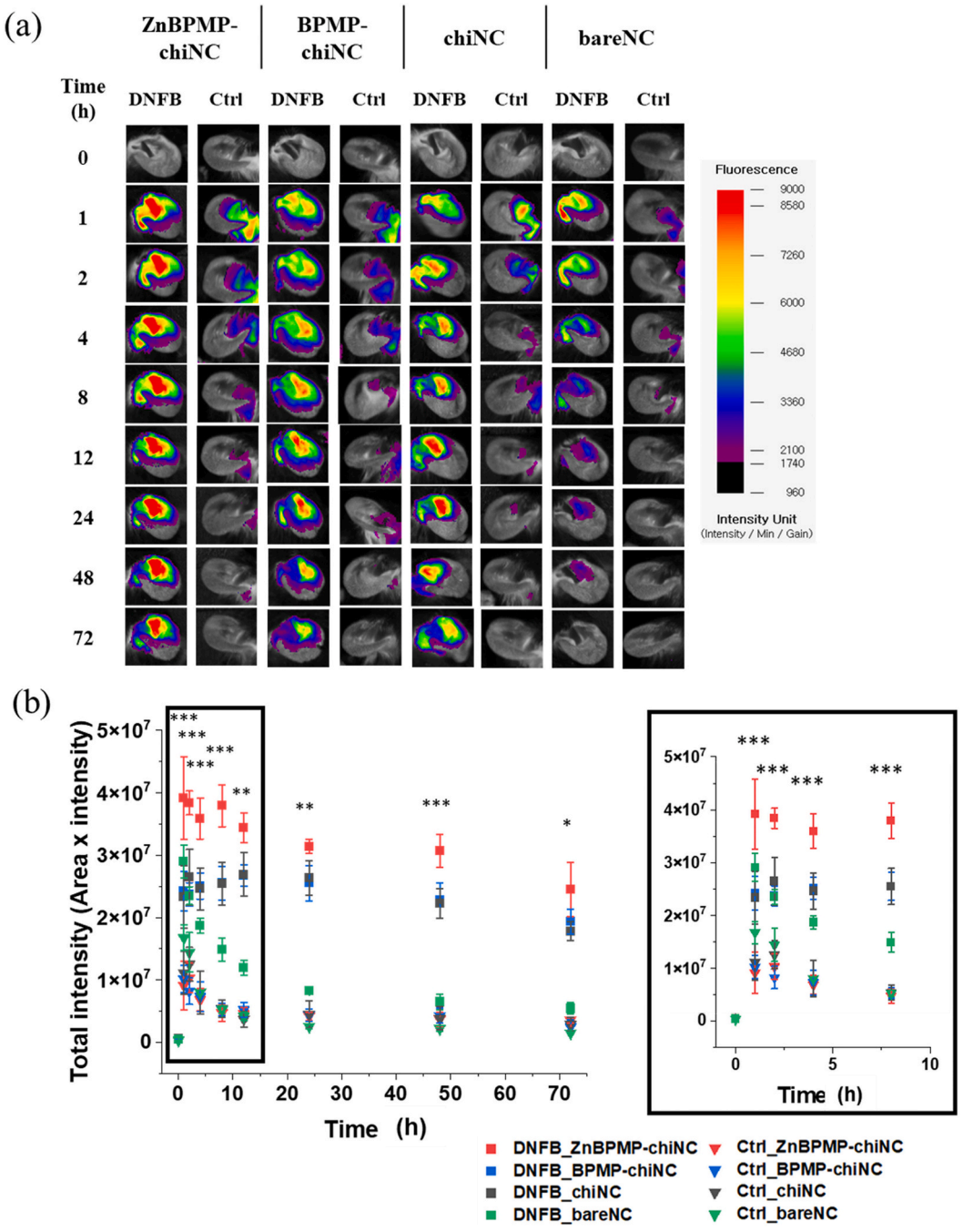

Fig. 5. Targeting of the nanocarriers to the DNFB treated ear and the control ear over time up to 72 h. (a) Fluorescent images of the nanocarriers in the ears upon *i.v.* injection (b) Total signal intensity of the nanocarriers from the fluorescent images ($n = 5$). (*: $p < 0.05$, **: $p < 0.01$, ***: $p < 0.001$).

First, the observed targeting effect of functionalization by chitosan and ZnBPMP to the inflammation site (DNFB treated ear) was maintained at day 5, too. The highest signal was observed from ZnBPMP-chiNC, followed by both BPMP-chiNC and chiNC with no difference between them, and a much lower signal was observed from bareNC at the inflamed ear.

Second, bareNC showed a very low signal not from the ears but also from all other organs compared to other chitosan functionalized nanocarriers, confirming a fast clearance rate of the nanocarrier itself without any surface modification *in vivo*, as expected from the time-course imaging of the ears (Fig. 5). In contrast, chitosan functionalization of the nanocarrier greatly increased the bioavailability of the nanocarrier. Much higher signals were observed not only from the ear but also from all of the analyzed organs by chitosan functionalization. Greatly enhanced bioavailability (prolonged circulation) of the nanocarrier by chitosan functionalization would significantly contribute to the inflammation targeting effect of the nanocarrier. Although this prolonged circulation of the nanocarrier by chitosan functionalization resulted in increased non-specific signals at the liver and spleen, the main clearance organ for nanosystems, as well as other organs, selectivity to inflammation at the same tissue (DNFB treated ear *vs.* control ear) was well maintained. No noticeable differences in the fluorescence signal were observed in the lung among chitosan functionalized nanocarriers, supporting the maintenance of similar colloidal stability *in vivo*. Interestingly, BPMP conjugation to chiNC led to substantially decreased signals at the liver and spleen in contrast to a slightly increased signal at

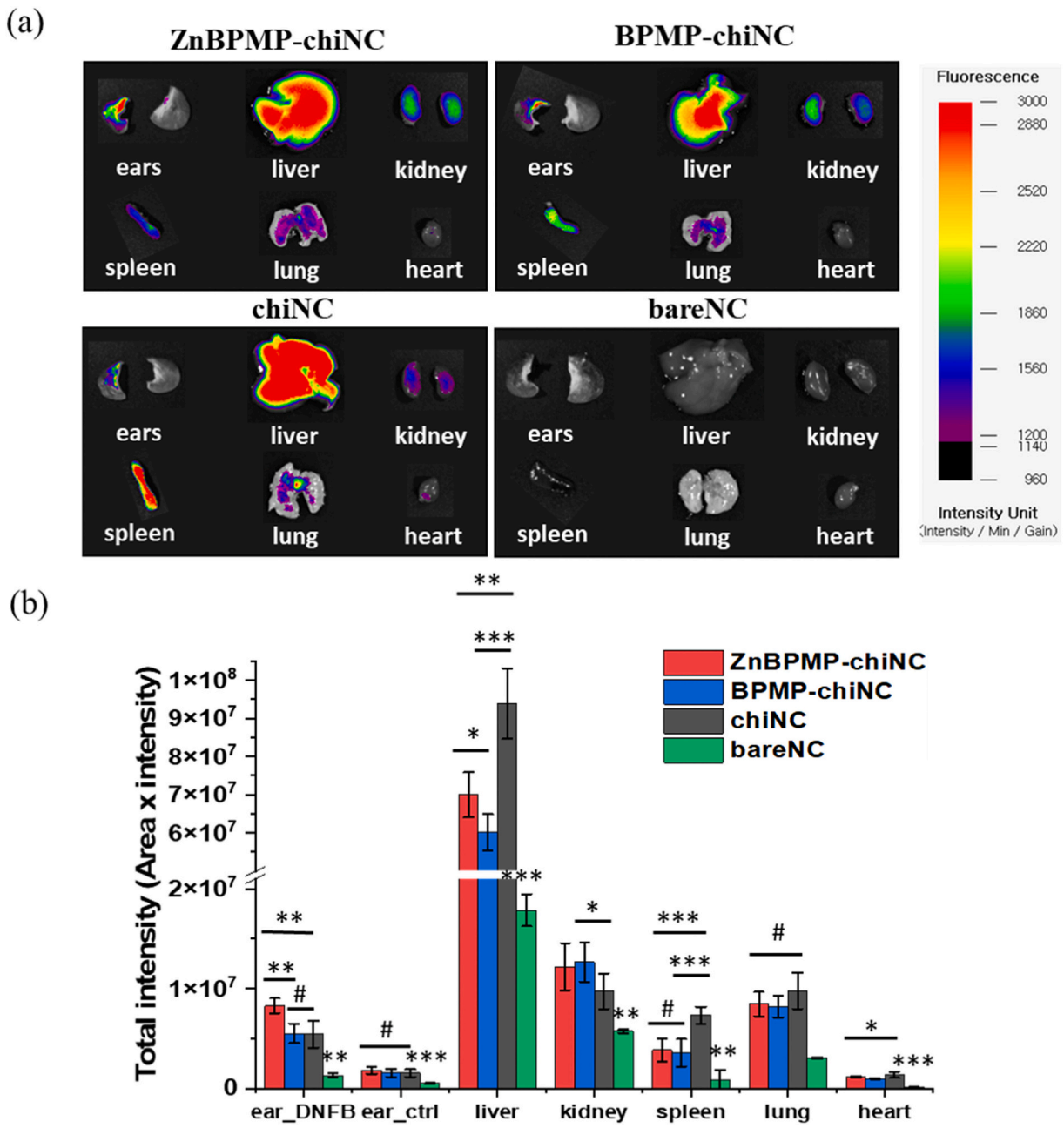

Fig. 6. Biodistribution of the nanocarriers on the ears and major organs *ex vivo* at day 5 after *i.v.* injection. (a) Fluorescent images of the nanocarriers accumulated in the major organs. The top side from left: ear_DNFB, ear_control, liver, and kidney. The bottom side from left: spleen, lung, and heart. (b) Total signal intensity from the ears and the major organs ($n = 5$). (*: $p < 0.05$, **: $p < 0.01$, ***: $p < 0.001$, $^{\#}$: $p > 0.05$).

the kidney compared to chiNC. The liver and spleen are the main two organs responsible for the clearance of nanoparticles [52]. Also, they have similar sinusoid structures in blood vessels unlike the kidney [53]. However, the reason for this tendency could not be elucidated. Furthermore, the chelation of Zn^{2+} ion did not affect significantly the biodistribution of the nanocarriers in the major organs in contrast to a distinct effect of the chelation Zn^{2+} ion on the inflammation targeting. So, the change in biodistribution among major organs by BPMP conjugation was not related to the specific affinity of ZnBPMP to PS, but due to the non-specific contribution of BPMP itself. Nonetheless, considering the dominance of the accumulation of the nanocarriers in the liver, ZnBPMP conjugation to chiNC contributed to a meaningful decrease in overall non-specific accumulation to the remaining body. Little accumulation was observed from the heart for all the groups, so the heart was not an important organ for the nanocarriers in terms of biodistribution.

Various inflammation-targeted drug delivery systems *in vivo* have been reported. However, in terms of targeting efficiency and longevity, previously reported ZnDPA systems using near-infrared (NIR) dye-conjugated ZnDPA itself for targeting acute muscular cell death and arthritis maintained their targeting signals less than 24 h [13,14]. Other polymer-based nanocarriers (PF68 and heparin-coated albumin) also remained at the inflamed colitis tissues for less than 24 h [54,55]. In the cases of other systems using specific targeting moiety for the inflammation, such as targeting macrophages or using leukocyte proteins, most of the systems were cleared out within 24 h [56,57], or less than 3 days [58]. In contrast, ZnBPMP-chiNC could maintain its targeting signal much higher than the control signal over 5 days. Considering the beneficial effect of the prolonged residence of a delivery carrier at the target site on therapeutic outcomes of delivered drugs, the present ZnBPMP-chiNC showed a significant advantage.

In summary, chitosan functionalization dramatically enhanced the *in vivo* circulation time of the nanocarriers for major organs, contributing to the continuous accumulation of them in the inflamed ear, so greatly enhanced the prolonged targeting ability of the nanocarrier to the inflamed ear was achieved. Additional ZnBPMP functionalization of the nanocarrier also resulted in significant improvement in the targeting of the inflamed ear in several aspects. First, ZnBPMP enhanced the initial targeting characteristic greatly; at 1 h, bareNC showed a higher signal than chiNC. However, ZnBPMP-chiNC showed much better initial targeting to the inflamed ear compared to bareNC or chiNC. Second, ZnBPMP further enhanced the targeting ability of chiNC to the inflamed ear up to 5 days, so the additional targeting effect of ZnBPMP was maintained. Third, BPMP conjugation decreased the overall non-specific accumulation of the nanocarrier to the remaining body.

In vitro cell experiments in Fig. 3 seemed to highlight the importance of ZnBPMP ligand for targeting the inflammation site. However, *in vivo* experiments revealed that both chitosan and ZnBPMP ligand are necessary for efficient targeting and prolonged remaining at the inflammation site. We previously reported the advantages of pluronic-based nanocarriers as an excellent delivery system with simple and efficient loading of various molecules as a bioactive state [32–35]. Thus, ZnBPMP-chiNC has a high potential applicable not only for the instant diagnosis of the inflammation site but also for the remedy of inflamed tissues and organs by delivering therapeutic agents better and longer. The therapeutic effect of drug-loaded nanocarriers needs to be evaluated using animal inflammation-associated disease models for further studies.

4. Conclusions

A novel nanocarrier system for effectively targeting the inflammation site was developed through the functionalization of chitosan and ZnBPMP moiety onto a pluronic-based nanocarrier. The system maintained its thermosensitivity, enabling efficient loading of drugs in a simple way. The targeting efficiencies of the nanocarriers with various surface modifications upon intravenous injection were analyzed using apoptosis-induced immune cells and an inflammation model in the mouse ear caused by skin hypersensitivity with DNFB. ZnBPMP moiety dramatically increased the cellular uptake and binding interaction with apoptosis-induced cells *in vitro*. Furthermore, it augmented the targeting efficiency and selectivity of the chitosan-functionalized nanocarrier from the beginning, and reduced non-specific accumulation in other organs, especially the liver and spleen *in vivo*. Chitosan functionalization could greatly prolong the *in vivo* circulation as well as the residence of the nanocarriers at the inflammation site. The developed system could maintain its targeting characteristics at the inflamed site until day 5 upon one-time injection. Thus, the present system in this study has the potential to be applied not only for targeting and imaging the disease site but also for delivering therapeutic drugs with high selectivity to the inflammation sites.

CRediT authorship contribution statement

Kiyoon Min: Methodology, Investigation, Formal analysis, Writing - Original Draft, Visualization

Soyeon Yoo: Methodology, Investigation, Formal analysis, Writing - Original Draft, Visualization

Min Su Han: Conceptualization, Validation, Writing - Review & Editing, Supervision

Giyoong Tae: Conceptualization, Resources, Writing - Review & Editing, Supervision, Funding acquisition

Declaration of competing interest

The authors declare that they have no known competing financial interests or personal relationships that could have appeared to influence the work reported in this paper.

Acknowledgements

This work was financially supported by NRF [2018R1A4A1024963 and 2021R1A2C2004722], Ministry of Science, ICT & Future Planning, Korea.

Appendix A. Supplementary data

Supplementary data to this article can be found online at https://doi.org/10.1016/j.msec.2021.112521.

References

[1] S.F. Moss, M.J. Blaser, Mechanisms of disease: inflammation and the origins of cancer, Nat. Rev. Clin. Oncol. 2 (2) (2005) 90–97.
[2] Y.J. Ko, J.-W. Lee, E.-J. Yang, N. Jang, J. Park, Y.K. Jeon, J.-W. Yu, N.-H. Cho, H.-S. Kim, I.C. Kwon, Non-invasive in vivo imaging of caspase-1 activation enables rapid and spatiotemporal detection of acute and chronic inflammatory disorders, Biomaterials 226 (2020), 119543.
[3] K. Jin, Z. Luo, B. Zhang, Z. Pang, Biomimetic nanoparticles for inflammation targeting, Acta Pharm. Sin. B 8 (1) (2018) 23–33.
[4] Y. Yang, Y. Ding, B. Fan, Y. Wang, Z. Mao, W. Wang, J. Wu, Inflammation-targeting polymeric nanoparticles deliver sparfloxacin and tacrolimus for combating acute lung sepsis, J. Control. Release 321 (2020) 463–474.
[5] C. Lautenschläger, C. Schmidt, C.-M. Lehr, D. Fischer, A. Stallmach, PEG-functionalized microparticles selectively target inflamed mucosa in inflammatory bowel disease, Eur. J. Pharm. Biopharm. 85 (3, Part A) (2013) 578–586.
[6] C. Li, H. Li, Q. Wang, M. Zhou, M. Li, T. Gong, Z. Zhang, X. Sun, pH-sensitive polymeric micelles for targeted delivery to inflamed joints, J. Control. Release 246 (2017) 133–141.
[7] H. Ren, Y. He, J. Liang, Z. Cheng, M. Zhang, Y. Zhu, C. Hong, J. Qin, X. Xu, J. Wang, Role of liposome size, surface charge, and PEGylation on rheumatoid arthritis targeting therapy, ACS Appl. Mater. Interfaces 11 (22) (2019) 20304–20315.
[8] H. Agarwal, A. Nakara, V.K. Shanmugam, Anti-inflammatory mechanism of various metal and metal oxide nanoparticles synthesized using plant extracts: a review, Biomed. Pharmacother. 109 (2019) 2561–2572.
[9] M.K. Shim, H.Y. Yoon, S. Lee, M.K. Jo, J. Park, J.-H. Kim, S.Y. Jeong, I.C. Kwon, K. Kim, Caspase-3/-7-specific metabolic precursor for bioorthogonal tracking of tumor apoptosis, Sci. Rep. 7 (1) (2017) 16635.
[10] G. Hu, M. Guo, J. Xu, F. Wu, J. Fan, Q. Huang, G. Yang, Z. Lv, X. Wang, Y. Jin, Nanoparticles targeting macrophages as potential clinical therapeutic agents against cancer and inflammation, Front. Immunol. 10 (1998) (2019).
[11] M. Kopf, M.F. Bachmann, B.J. Marsland, Averting inflammation by targeting the cytokine environment, Nat. Rev. Drug Discov. 9 (9) (2010) 703–718.
[12] B.A. Smith, W.J. Akers, W.M. Leevy, A.J. Lampkins, S. Xiao, W. Wolter, M. A. Suckow, S. Achilefu, B.D. Smith, Optical imaging of mammary and prostate tumors in living animals using a synthetic near infrared Zinc(II)-dipicolylamine probe for anionic cell surfaces, J. Am. Chem. Soc. 132 (1) (2010) 67–69.
[13] M.M. Chan, B.D. Gray, K.Y. Pak, D. Fong, Non-invasive in vivo imaging of arthritis in a collagen-induced murine model with phosphatidylserine-binding near-infrared (NIR) dye, Arthritis Res. Ther. 17 (1) (2015) 50.
[14] B.A. Smith, S.T. Gammon, S. Xiao, W. Wang, S. Chapman, R. McDermott, M. A. Suckow, J.R. Johnson, D. Piwnica-Worms, G.W. Gokel, B.D. Smith, W.M. Leevy, In vivo optical imaging of acute cell death using a near-infrared fluorescent Zinc−Dipicolylamine probe, Mol. Pharm. 8 (2) (2011) 583–590.
[15] Y.-W. Liu, K.-S. Shia, C.-H. Wu, K.-L. Liu, Y.-C. Yeh, C.-F. Lo, C.-T. Chen, Y.-Y. Chen, T.-K. Yeh, W.-H. Chen, J.-J. Jan, Y.-C. Huang, C.-L. Huang, M.-Y. Fang, B.D. Gray, K.Y. Pak, T.-A. Hsu, K.-H. Huang, L.K. Tsou, Targeting tumor associated phosphatidylserine with new zinc dipicolylamine-based drug conjugates, Bioconjug. Chem. 28 (7) (2017) 1878–1892.
[16] H.D. Lu, S.S. Yang, B.K. Wilson, S.A. McManus, C.V.H.H. Chen, R.K. Prud'homme, Nanoparticle targeting of Gram-positive and Gram-negative bacteria for magnetic-based separations of bacterial pathogens, Appl. Nanosci. 7 (3) (2017) 83–93.
[17] H. Zhao, P. Zhou, K. Huang, G. Deng, Z. Zhou, J. Wang, M. Wang, Y. Zhang, H. Yang, S. Yang, Amplifying apoptosis homing nanoplatform for tumor theranostics, Adv. Healthc. Mater. 7 (14) (2018) 1800296.
[18] Y. Lee, S. Yoo, S. Kang, S. Hong, M.S. Han, An [Mn2(bpmp)]3+ complex as an artificial peroxidase and its applications in colorimetric pyrophosphate sensing and cascade-type pyrophosphatase assay, Analyst 143 (8) (2018) 1780–1785.
[19] S. Yoo, K. Min, G. Tae, M.S. Han, A long-term stable paper-based glucose sensor using a glucose oxidase-loaded, Mn2BPMP-conjugated nanocarrier with a smartphone readout, Nanoscale 13 (8) (2021) 4467–4474.
[20] S.K. Kim, D.H. Lee, J.-I. Hong, J. Yoon, Chemosensors for pyrophosphate, Acc. Chem. Res. 42 (1) (2009) 23–31.
[21] S. Lee, K.K.Y. Yuen, K.A. Jolliffe, J. Yoon, Fluorescent and colorimetric chemosensors for pyrophosphate, Chem. Soc. Rev. 44 (7) (2015) 1749–1762.
[22] M.S. Han, D.H. Kim, Naked-eye detection of phosphate ions in water at physiological pH: a remarkably selective and easy-to-assemble colorimetric phosphate-sensing probe, Angew. Chem. Int. Ed. 41 (20) (2002) 3809–3811.

[23] D.H. Lee, J.H. Im, S.U. Son, Y.K. Chung, J.-I. Hong, An azophenol-based chromogenic pyrophosphate sensor in water, J. Am. Chem. Soc. 125 (26) (2003) 7752–7753.
[24] H. Jiang, E.J. O'Neil, K.M. DiVittorio, B.D. Smith, Anion-mediated phase transfer of Zinc(II)-coordinated tyrosine derivatives, Org. Lett. 7 (14) (2005) 3013–3016.
[25] A. Ojida, Y. Mito-oka, M.-A. Inoue, I. Hamachi, First artificial receptors and chemosensors toward phosphorylated peptide in aqueous solution, J. Am. Chem. Soc. 124 (22) (2002) 6256–6258.
[26] A. Ojida, Y. Mito-oka, K. Sada, I. Hamachi, Molecular recognition and fluorescence sensing of monophosphorylated peptides in aqueous solution by Bis(zinc(II)−dipicolylamine)-based artificial receptors, J. Am. Chem. Soc. 126 (8) (2004) 2454–2463.
[27] H.-W. Rhee, H.-Y. Choi, K. Han, J.-I. Hong, Selective fluorescent detection of flavin adenine dinucleotide in human eosinophils by using Bis(Zn2+-Dipicolylamine) complex, J. Am. Chem. Soc. 129 (15) (2007) 4524–4525.
[28] E.J. O'Neil, B.D. Smith, Anion recognition using dimetallic coordination complexes, Coord. Chem. Rev. 250 (23) (2006) 3068–3080.
[29] W.I. Choi, G. Tae, Y.H. Kim, One pot, single phase synthesis of thermo-sensitive nano-carriers by photo-crosslinking of a diacrylated pluronic, J. Mater. Chem. 18 (24) (2008) 2769–2774.
[30] P. Zarrintaj, J.D. Ramsey, A. Samadi, Z. Atoufi, M.K. Yazdi, M.R. Ganjali, L. M. Amirabad, E. Zangene, M. Farokhi, K. Formela, M.R. Saeb, M. Mozafari, S. Thomas, Poloxamer: a versatile tri-block copolymer for biomedical applications, Acta Biomater. 110 (2020) 37–67.
[31] E. Russo, C. Villa, Poloxamer hydrogels for biomedical applications, Pharmaceutics 11 (12) (2019).
[32] W.I. Choi, Y.H. Kim, G. Tae, Controlled release of proteins from pluronic-based nano-carrier, Macromol. Res. 19 (6) (2011) 639–642.
[33] M. Kim, A. Sahu, Y. Hwang, G.B. Kim, G.H. Nam, I.-S. Kim, I. Kwon, G. Tae, Targeted delivery of anti-inflammatory cytokine by nanocarrier reduces atherosclerosis in apo E−/- mice, Biomaterials 226 (2020), 119550.
[34] J.-Y. Kim, W.I. Choi, M. Kim, G. Tae, Tumor-targeting nanogel that can function independently for both photodynamic and photothermal therapy and its synergy from the procedure of PDT followed by PTT, J. Control. Release 171 (2) (2013) 113–121.
[35] S. Kim, M. Kim, S. Jung, K. Kwon, J. Park, S. Kim, I. Kwon, G. Tae, Co-delivery of therapeutic protein and catalase-mimic nanoparticle using a biocompatible nanocarrier for enhanced therapeutic effect, J. Control. Release 309 (2019) 181–189.
[36] J.-Y. Kim, W.I. Choi, Y.H. Kim, G. Tae, S.-Y. Lee, K. Kim, I.C. Kwon, In-vivo tumor targeting of pluronic-based nano-carriers, J. Control. Release 147 (1) (2010) 109–117.
[37] W.I. Choi, J.H. Lee, J.-Y. Kim, J.-C. Kim, Y.H. Kim, G. Tae, Efficient skin permeation of soluble proteins via flexible and functional nano-carrier, J. Control. Release 157 (2) (2012) 272–278.
[38] J.-Y. Kim, W.I. Choi, Y.H. Kim, G. Tae, Highly selective in-vivo imaging of tumor as an inflammation site by ROS detection using hydrocyanine-conjugated, functional nano-carriers, J. Control. Release 156 (3) (2011) 398–405.
[39] J.-Y. Kim, W.I. Choi, Y.H. Kim, G. Tae, Brain-targeted delivery of protein using chitosan- and RVG peptide-conjugated, pluronic-based nano-carrier, Biomaterials 34 (4) (2013) 1170–1178.
[40] J.H. Lee, A. Sahu, W.I. Choi, J.Y. Lee, G. Tae, ZOT-derived peptide and chitosan functionalized nanocarrier for oral delivery of protein drug, Biomaterials 103 (2016) 160–169.
[41] D.J. Oh, K.M. Kim, K.H. Ahn, Nanoparticle-based indicator-displacement assay for pyrophosphate, Chem. Asian J. 6 (8) (2011) 2034–2039.
[42] W.I. Choi, J.-Y. Kim, C. Kang, C.C. Byeon, Y.H. Kim, G. Tae, Tumor regression in vivo by photothermal therapy based on gold-nanorod-loaded, functional nanocarriers, ACS Nano 5 (3) (2011) 1995–2003.
[43] R.G. Hanshaw, C. Lakshmi, T.N. Lambert, J.R. Johnson, B.D. Smith, Fluorescent detection of apoptotic cells by using zinc coordination complexes with a selective affinity for membrane surfaces enriched with phosphatidylserine, ChemBioChem 6 (12) (2005) 2214–2220.
[44] M.A. Moro-García, J.C. Mayo, R.M. Sainz, R. Alonso-Arias, Influence of inflammation in the process of T lymphocyte differentiation: proliferative, metabolic, and oxidative changes, Front. Immunol. 9 (339) (2018).
[45] M. Bonneville, C. Chavagnac, M. Vocanson, A. Rozieres, J. Benetiere, I. Pernet, A. Denis, J.-F. Nicolas, A. Hennino, Skin contact irritation conditions the development and severity of allergic contact dermatitis, J. Investig. Dermatol. 127 (6) (2007) 1430–1435.
[46] W.I. Choi, N. Kamaly, L. Riol-Blanco, I.-H. Lee, J. Wu, A. Swami, C. Vilos, B. Yameen, M. Yu, J. Shi, I. Tabas, U.H. von Andrian, S. Jon, O.C. Farokhzad, A solvent-free thermosponge nanoparticle platform for efficient delivery of labile proteins, Nano Lett. 14 (11) (2014) 6449–6455.
[47] J. Key, K. Park, Multicomponent, tumor-homing chitosan nanoparticles for cancer imaging and therapy, Int. J. Mol. Sci. 18 (3) (2017).
[48] J.H. Na, H. Koo, S. Lee, S.J. Han, K.E. Lee, S. Kim, H. Lee, S. Lee, K. Choi, I.C. Kwon, K. Kim, Precise targeting of liver tumor using glycol chitosan nanoparticles: mechanisms, key factors, and their implications, Mol. Pharm. 13 (11) (2016) 3700–3711.
[49] A. Punnia-Moorthy, Evaluation of pH changes in inflammation of the subcutaneous air pouch lining in the rat, induced by carrageenan, dextran and staphylococcus aureus, J. Oral Pathol. Med. 16 (1) (1987) 36–44.
[50] P. Rajitha, D. Gopinath, R. Biswas, M. Sabitha, R. Jayakumar, Chitosan nanoparticles in drug therapy of infectious and inflammatory diseases, Expert Opin. Drug Deliv. 13 (8) (2016) 1177–1194.
[51] J.S. Pober, W.C. Sessa, Inflammation and the blood microvascular system, Cold Spring Harb. Perspect. Biol. 7 (1) (2015).
[52] K.M. Tsoi, S.A. MacParland, X.-Z. Ma, V.N. Spetzler, J. Echeverri, B. Ouyang, S. M. Fadel, E.A. Sykes, N. Goldaracena, J.M. Kaths, J.B. Conneely, B.A. Alman, M. Selzner, M.A. Ostrowski, O.A. Adeyi, A. Zilman, I.D. McGilvray, W.C.W. Chan, Mechanism of hard-nanomaterial clearance by the liver, Nat. Mater. 15 (11) (2016) 1212–1221.
[53] J.C. Kim, G. Tae, The modulation of biodistribution of stem cells by anchoring lipid-conjugated heparin on the cell surface, J. Control. Release 217 (2015) 128–137.
[54] X. Wang, J.-J. Yan, L. Wang, D. Pan, R. Yang, Y. Xu, J. Sheng, Q. Huang, H. Zhao, M. Yang, Rational design of polyphenol-poloxamer nanovesicles for targeting inflammatory bowel disease therapy, Chem. Mater. 30 (12) (2018) 4073–4080.
[55] S. Zhang, W.J. Cho, A.T. Jin, L.Y. Kok, Y. Shi, D.E. Heller, Y.-A.L. Lee, Y. Zhou, X. Xie, J.R. Korzenik, J.K. Lennerz, G. Traverso, Heparin-coated albumin nanoparticles for drug combination in targeting inflamed intestine, Adv. Healthc. Mater. 9 (16) (2020) 2000536.
[56] Y. Zhao, Y. Yang, J. Zhang, R. Wang, B. Cheng, D. Kalambhe, Y. Wang, Z. Gu, D. Chen, B. Wang, Y. Huang, Lactoferrin-mediated macrophage targeting delivery and patchouli alcohol-based therapeutic strategy for inflammatory bowel diseases, Acta Pharm. Sin. B 10 (10) (2020) 1966–1976.
[57] A. Zinger, M. Sushnitha, T. Naoi, G. Baudo, E. De Rosa, J. Chang, E. Tasciotti, F. Taraballi, Enhancing inflammation targeting using tunable leukocyte-based biomimetic nanoparticles, ACS Nano 15 (4) (2021) 6326–6339.
[58] N.G. Deane, H.C. Manning, A.C. Foutch, M.K. Washington, B.A. Aronow, D. J. Bornhop, R.J. Coffey, Targeted imaging of colonic tumors in Smad3−/− mice discriminates cancer and inflammation, Mol. Cancer Res. 5 (4) (2007) 341.